Laser-induced Fluorescence Analysis of HNO Generated from the Thermal Decomposition of Hydroxylammonium Nitrate

N.R. Taylor and K.M. Lemmer
Western Michigan University
Kalamazoo, MI

ABSTRACT

The ionic liquid hydroxylammonium nitrate (HAN) is a promising propellant for various types of spacecraft propulsion including chemical monopropellants, electrospray thrusters, and field reversed configuration thrusters. With regards to plasma-based electric propulsion applications, the ionic liquid is thermally and/or catalytically decomposed into a vapor and subsequently injected for ionization. Among the various species generated from HAN decomposition is the formation of nitroxyl (HNO), an important molecule with implications in both chemical and electric propulsion applications. Previous low pressure HAN decomposition studies utilized a heated capillary to generate the decomposition vapor, and a mass spectrometer positioned in-line with the vacuum system detected HNO. Unfortunately, the fragmentation of various N-O containing molecules generated from the decomposition process complicates data analysis and introduces uncertainty in the results. To overcome this experimental challenge a laser-induced fluorescence (LIF) chamber has been inserted into our existing experimental platform. The highly selective and sensitive nature of LIF provides a direct means of detecting HNO generated from HAN decomposition within a low pressure environment. A single-mode dye laser was used to examine two excitation transitions: the $\tilde{A}\ ^1A'' \leftarrow X\ ^1A'$ (100 – 000), K' = 1 – K'' = 0 ro-vibrational transition at λ = 623.8 nm and the $\tilde{A}\ ^1A'' \leftarrow X\ ^1A'$ (011 – 000), K' = 1 – K'' = 0 ro-vibrational transition at λ = 642.3 nm. The resulting fluorescence photons were detected with a high-resolution spectrometer. Analysis on the production of HNO will be discuss with respect to background gas pressure and thermal decomposition temperature.

INTRODUCTION

Ionic liquids (ILs) have emerged in recent years as potential "green" monopropellants for chemical propulsion with interest in a dual-mode propellant replacement in electric propulsion devices.[1,2] In addition to being environmentally benign, ILs tend to be chemically stable and exhibit low-toxicity. Due to very strong intramolecular interactions (ion-dipole, dipole-dipole, and hydrogen bonding) IL densities are relatively high and their vapor pressures are extremely low. As a result they have been widely utilized as propellants in electrospray thrusters.[3–12] Moreover, ILs are known to thermally decompose into gas phase species which can be utilized in gas-fed electric propulsion devices.[2,13–31] In order to maximize the propellant's utility, the parameters that influence chemical composition of the emitted gas phase species must be well characterized.

One particular IL that has received notable attention is hydroxylammonium nitrate (HAN). In 1985 Cronin and Brill examined the decomposition of HAN and speculated that the initial reaction involved proton transfer from the hydroxylammonium ion (NH_3OH^+) to the nitrate ion (NO_3^-) to form hydroxylamine (NH_2OH) and nitric acid (HNO_3).[31] They postulated that hydroxylamine would further degrade into nitrous oxide (N_2O) and ammonia (NH_3). In 1988 Oxley and Brower conducted a comprehensive chemical gas analysis on the thermal decomposition of HAN and proposed several chemical mechanisms for the generation and reaction of observed species.[23] Among these species was nitroxyl, HNO, which they treated as both a product of HAN decomposition, and a reactant for subsequent chemical reactions. Included in their mechanisms were reactions involving the formation of nitrous oxide as a final product. Later studies by Schoppelrei and Brill would examine the production of nitrous oxide as a product of the dimerization of nitroxyl produced from HAN decomposition under high pressure conditions.[32]

Air Force Office of Scientific Research Grant FA9550-18-1-0442

In recent years there have been a number of computational studies examining the decomposition of hydroxylamine.[33–35] Most notable is the extensive study conducted by Izato *et al.* where they examined the early decomposition pathways of hydroxylamine in aqueous solutions.[35] Based on their computational analysis they concluded that a cation-catalyzed reaction was the likely initial decomposition pathway, as shown in reactions R1-R6, with R6 being the overall reaction.

R1. $NH_3OH^+ + NO_3^- \rightarrow NH_2OH + HNO_3$

R2. $NH_2OH + NH_2OH + NH_3OH^+ \rightarrow NH_2NH_2OH^+ + NH_2OH + H_2O$

R3. $NH_2NH_2OH^+ \rightarrow NH_3NH_2O^+$

R4. $NH_3NH_2O^+ \rightarrow NH_4^+ + HNO$

R5. $NH_4^+ + NH_2OH \rightarrow NH_3OH^+ + NH_3$

R6. $\mathbf{NH_2OH + NH_2OH \rightarrow NH_3 + HNO + H_2O}$

Despite nitroxyl being predicted as a decomposition product of HAN, there have been no direct experimental observations of HNO, rather, its production has been implied due to the subsequent formation and detection of nitrous oxide. The objective of this research is to experimentally assess the validity of laser-induced fluorescence spectroscopy as a means to directly observe the production of HNO from the thermal decomposition of HAN. We will assess two possible excitation schemes. The first involving the $\tilde{A}^1A'' - X^1A'$ (100 – 000) transition at 623.8 nm and the second involving the $\tilde{A}^1A'' - X^1A'$ (011 – 000) transition at 642.3 nm. Further assessment will be made by examining the excitation profiles of the 623.8 nm transition. Laser-induced saturation conditions will also be examined. Finally, the influence of the background gas pressure on the HNO fluorescence signal will be discussed. The results obtained from this research effort are a first step toward the direct quantitative detection of nitroxyl produced from the decomposition of HAN. Furthermore, this research has wide analytical implications. The highly reactivity nature of the HNO radical does not allow the development of analytical standards, making quantitative measurements very challenging. The development of a method in which quantitative measurements of HNO can be made has applicability in the fields of atmospheric chemistry, combustion, and biomedical research.[36–41] Ultimately, the results obtained from this research effort will aid in the validation of computational modeling efforts as well as assist application researchers in the optimization of gas-phase electric propulsion thruster designs which utilize HAN as a propellant.

EXPERIMENTAL DESIGN

THERMAL DECOMPOSITION SYSTEM

An illustration of the experimental system used to examine the production of nitroxyl is shown in figure 1. Controlled quantities of HAN are injected into the thermal decomposition system by controlling the pressure differential between the vacuum chamber and liquid reservoirs. The thermal decomposition system is evacuated to a base pressure of 65 mTorr, and a mass flow controller allows direct control of the back pressure exerted on the liquid reservoirs, facilitating active control of the liquid flow rate through the system. An automated 3-way valve is used to select which liquid is injected into the chamber. Water is used here to flush the system when necessary and assess background signal levels. A liquid flow meter positioned in-line with the capillary system is used to measure the flow rate of liquid delivered to the thermal

Air Force Office of Scientific Research Grant FA9550-18-1-0442

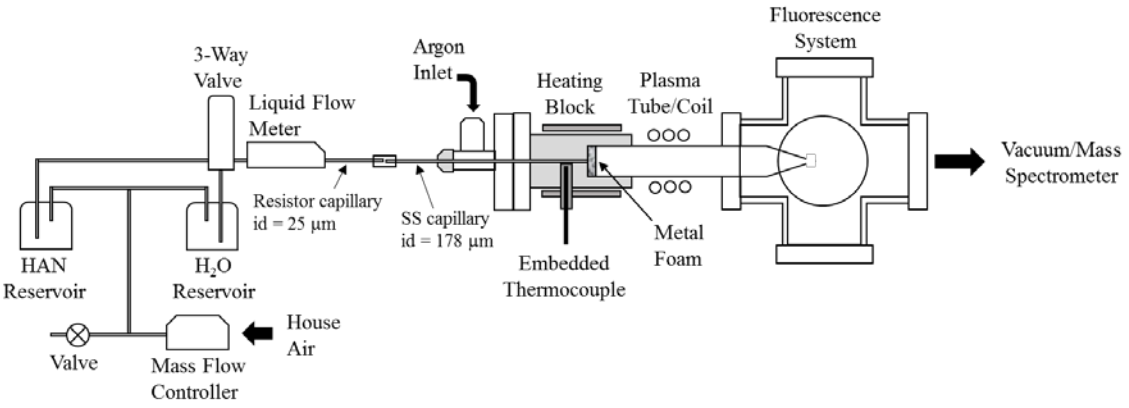

Figure 1: Illustration of the experimental platform used for thermal decomposition and plasma excitation of ionic liquid propellants.

decomposition system. The liquid emerging from the flow meter flows through a fused silica capillary with an inner diameter of 25 μm which restricts the flow and allows more precise control of the flow rate. The resulting liquid is injected into a stainless-steel capillary with an inner diameter of 178 μm (0.007”), an outer diameter of 4.76 mm (3/16”), and length of 200 mm. The final 50 mm portion of the stainless-steel capillary is confined within an aluminum heating block at a temperature that is controlled with thermal tape. Four embedded K-type thermocouples positioned along the heating block (only one shown) are used to acquire temperature measurements along the heated portion of the capillary. Immediately following the end of the heated capillary are two sintered stainless-steel disks. The first has a porosity of 100 μm, and the second disk has a porosity of 10 μm. The purpose of the stainless-steel disks is to homogenize the gas vapor that emerges from the capillary, providing a fairly uniform distribution of vaporized species. An additional feature of these metal disks is the potential for catalytic studies; although, no catalytic studies have been conducted with this experimental setup. The gas vapor emerging from the metal disks flows through a 20.3 cm (8”) long fused quartz tube with an outer diameter of 25.8 mm and inner diameter of 22 mm. The end of the fused quartz tube has been tapered to a final inner diameter of 5 mm in order to funnel and focus the gas species into the LIF chamber and increase the density in the laser probed volume. A mass spectrometer was positioned further downstream.

LASER-INDUCED FLUORESCENCE SYSTEM

The laser-induced fluorescence system is constructed of a 6-way 2.75-inch con-flat flange cube fitted with viewports with anti-reflection coated windows. An illustration of the optical system is shown in figure 2. A single-mode cw dye laser with a linewidth of ~250 kHz was used as the excitation source. A Fresnel rhomb was used to control the polarization orientation of the beam, and beam steering optics directed and focused the beam into the fluorescence chamber. A lens and mirror system collimated and reflected the beam back into the system, effectively doubling the incident power on the gas species emerging from the quartz tube. Fluorescence photons were collected orthogonal to the incident beam with a two lens system with focal lengths chosen to match the f-number of the spectrometer. A second lens and mirror system were also used in order to double the collection solid angle. The resulting fluorescent photons were detected with a high-resolution spectrometer equipped with a cooled CCD detector.

Air Force Office of Scientific Research Grant FA9550-18-1-0442

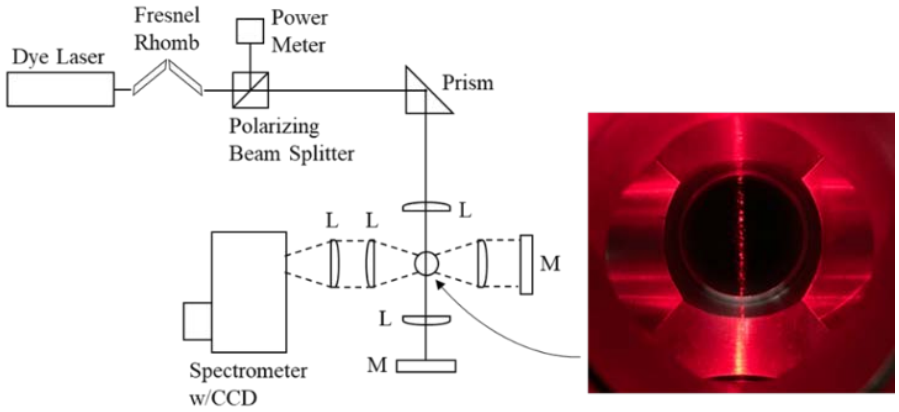

RESULTS AND DISCUSSION

Figure 2: Illustration of the optical excitation and detection system. An image of the fluorescence chamber with the laser beam is shown.

MASS SPECTROMETRY OF NITROXYL (HNO)

Initially we examined the possibility of using mass spectrometry as the detection method for nitroxyl, HNO. As illustrated in R1, nitric acid, HNO_3, is expected to be vaporized in significant quantities when HAN is thermally decomposed. The molecular form of nitric acid easily fragments by electron impact ionization, forming substantial ion fragments at m/z = 46 (NO_2^+), m/z = 30 (NO^+), m/z = 16 ($^{16}O^+$), and m/z = 14 ($^{14}N^+$). Since nitroxyl contains both nitrogen and oxygen, spectral overlap is realized. Therefore, to selectively detect the production of nitroxyl from the thermal decomposition of HAN, detection of the molecular form of nitroxyl at m/z = 31 is required.

HAN was introduced into the thermal decomposition system and the resulting gas was analyzed with a mass spectrometer. After an extensive survey of the experimental parameters, it was found that a mass spectrometer electron impact energy of 25 eV, decomposition temperature of 433 K, and a flow rate approaching 1 μL/s resulted in the detection of nitroxyl at m/z = 31 as shown in figure 3. The small signal at m/z = 31 is due to the large degree at which HNO fragments into NO^+ and H^+. Moreover, the molecular ion of nitroxyl could only be detected under these extreme conditions, which represent an unfavorable set of experimental parameters. First, the system could only be operated under these conditions for a few minutes at a time in order to avoid contamination of the mass spectrometer. Second, the flow rate is unrealistic for spacecraft propulsion applications due to the high propellant consumption rate.

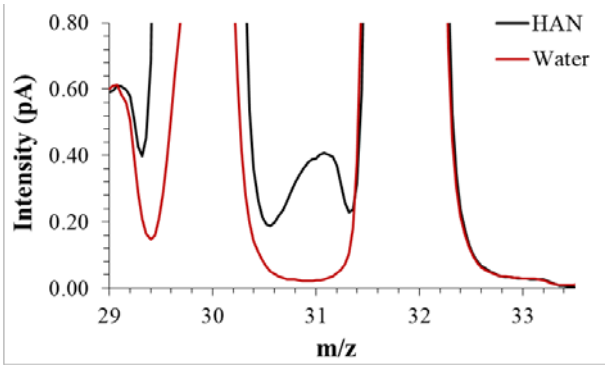

Figure 3: Mass spectrum of thermally decomposed HAN (black) and water (red). Four peaks are shown; m/z = 29 ($^{15}N^{14}N^+$), m/z = 30 (NO^+ = fragment ions from electron impact dissociation of HNO and HNO_3), m/z = 31 (HNO^+), m/z = 32 (O_2^+). Intensity is plotted in picoamps (pA).

Air Force Office of Scientific Research Grant FA9550-18-1-0442

These initial observations on the detection of nitroxyl suggest that mass spectrometry, which utilizes hard ionization techniques such as electron impact ionization, is insufficiently sensitive for the detection of HNO. Therefore, laser-induced fluorescence spectroscopy was explored as a possible method for the sensitive and selective detection of nitroxyl.

LASER-INDUCED FLUORESCENCE OF NITROXYL (HNO)

The first comprehensive spectroscopic analysis of HNO was conducted by Dalby in 1958.[42] Later works by Ramsay[43] and Dixon[44–46] expanded on this early work and provided a roadmap for which LIF analysis would be conducted. Based on these early works, as well as other reports,[41,44,47–52] two transitions were selected for investigation. The first involves the $\tilde{A}^1A'' - X^1A'$ (100 – 000) transition with excitation at 623.8 nm. The second involves the $\tilde{A}^1A'' - X^1A'$ (011 – 000) transition with laser excitation at 642.3 nm. The standard (ν_1, ν_2, ν_3) formalism used here represents the vibrational modes ν_1 (N-H stretching), ν_2 (N=O stretching), and ν_3 (H-N=O bending).

HAN was injected into the thermal decomposition system with the heating block set to a temperature of 417 K at a flow rate of approximately 80 nL/s. The resulting LIF spectra are shown in figure 4 with excitation at 624 nm on top and excitation at 642 nm on the bottom. Each of the laser excitation transitions exhibited three spectral regions of fluorescence. The lower wavelength fluorescence signals (figure 4-left), display a weak and noticeably broadened fluorescence spectrum relative to the other two higher wavelength spectra. The broadening of these spectral features is most likely attributed to a pre-dissociation mechanism involving the upper vibrational energy levels associated with these fluorescence transitions.[51] The primary fluorescence signals for 624 nm excitation were found in the 750 nm region (figure 4-top-middle) representing the $X\ ^1A'' \rightarrow X\ ^1A'$ (000 – 000) system. As for 642 nm excitation, the $X\ ^1A'' \rightarrow X\ ^1A'$ (000 – 001) fluorescence system centered around 715 nm (figure 4-bottom-middle) yielded the maximum fluorescence signal. Therefore, these two excitation and fluorescence schemes were chosen for further analysis of the detection of HNO. Finally, it should be noted that no observable fluorescence signal was detected when the laser was detuned 4 GHz from their respective transitions, further confirming the signals are resonant transitions of HNO.

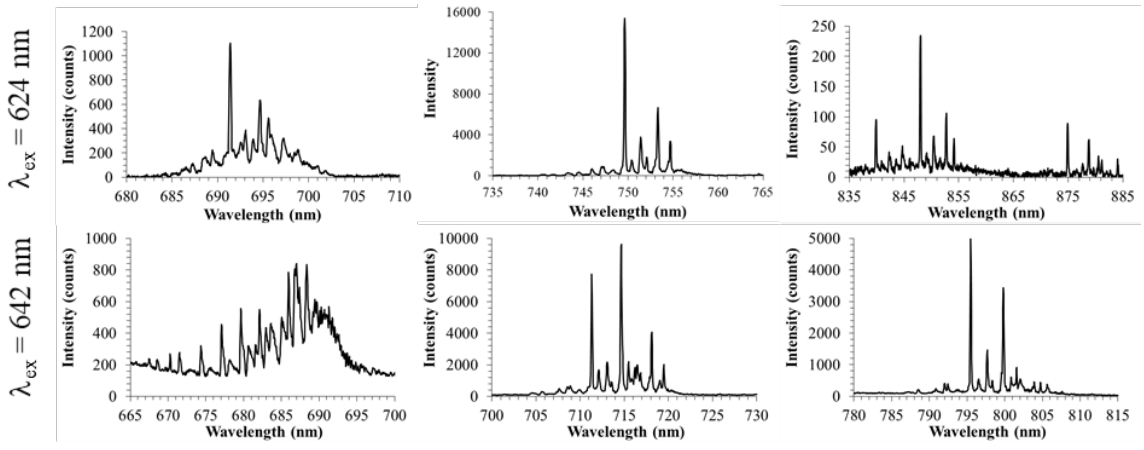

Figure 4: HNO fluorescence spectra from 624 nm excitation (top) and 642 nm excitation (bottom). Identical experimental parameters were utilized for the collection of these spectra.

NITROXYL FLUORESCENCE EXCITATION PROFILES AT 623.8 NM

The ultimate goal of the current study is to quantify of the amount of HNO generated based on various thermal decompostion parameters. From an experimental perspective, it would be ideal to tune the laser to the center of the HNO absorption profile and collect the resuting fluorescence under various experimental conditions. In order for the fluorscence signal to truly

Air Force Office of Scientific Research Grant FA9550-18-1-0442

represent the density of generated HNO, the absorption linewidth must remain fairly constant regardless of the upstream thermal decomposition parameters. Deviation from this assumption requires knowedge of the absorption linewidth for accurate quantification. In order to evaluate the validity of a near constant HNO absorption linewidth within the probed volume of the fluorescence chamber, fluorescence excitation profiles were acquired for a set of temperatures and background pressures. The dye laser utilized for HNO excitation was scanned 8 GHz over the Ã ^{1}A" ← X ^{1}A' (100 – 000), K' = 1 – K'' = 0 ro-vibrational transition. The scan time was 625 s per profile with a fluoresence spectra collected every 2.50 s, yeilding 250 data points per profile. Three scans were recorded per set of conditions. Each recorded fluorescence spectra was numerically integrated using Simpsons rule from 740 nm to 765 nm, which according to figure 4 (top-middle), constitued all of the signal for this fluorscence system. The resulting excitation profiles were normalized to the peak of the profile and are shown in figure 5. For visual clarity the 500 mTorr, 403 K and 500 mTorr, 443 K profiles have been shifted vertically by 0.2 and 0.4, respectively.

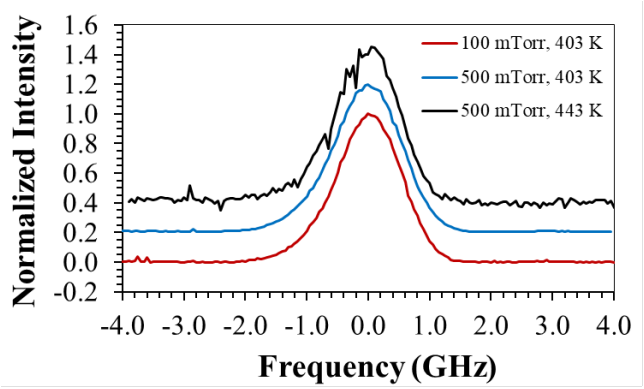

Figure 5: Fluorescence excitation profiles of the the Ã ^{1}A" ← X ^{1}A' (100 – 000), K' = 1 – K'' = 0 ro-vibrational transition at 624 nm.

The fluorescence excitation profiles in figure 5 indicate that the upstream thermal decompostion temperature does not significantly broaden the HNO absorption profile. Furthermore, increasing the background gas pressure also does not induce significant pressure broadening of the HNO excitation profile, as would be expected given the relatively small increase in gas pressure. Therefore, the assumpiton of a near constant absorption linewidth of HNO at the downstream probed volume for various thermal decompositon parameters has been experimentally validated. As a consequence, the resulting fluorescence signal with the laser tuned to the peak of the transitions can be considered representative of the density of HNO within the laser probed volume.

LASER-INDUCED FLUORESCENCE SATURATION CURVE FOR NITROXYL (HNO)

The magnitude of a molecular fluorescence signal is directly related to the amount of energy deposited into the system, with the signal increasing linearly until the onset of saturation. From an analytical perspective, it is ideal to saturate the probed transition since at this condition the maximum fluorescence signal is produced and it is independent of laser intensity fluctuations, yielding an optimal system signal-to-noise ratio. Therefore, assessment of saturation conditions was evaluated for thermally decomposed HAN at a temperature of 415 K with a system background pressure of 100 mTorr. Results from the analysis conducted on the 624 nm excitation transition and 750 nm fluorescence system are shown in figure 6. These results indicate the system begins to saturate at ~70 mWatts of incident power. Therefore, the laser was maintained at an output power of approximately 80 mWatts. A similar analysis was conducted on the 642 nm excitation transition while measuring the 715 nm fluorescence. Since 642 nm is in the middle of the tuning curve for the dye utilized (DCM) a power of ~150 mW was available and proved to be more than sufficient to optically saturate the transition.

Air Force Office of Scientific Research Grant FA9550-18-1-0442

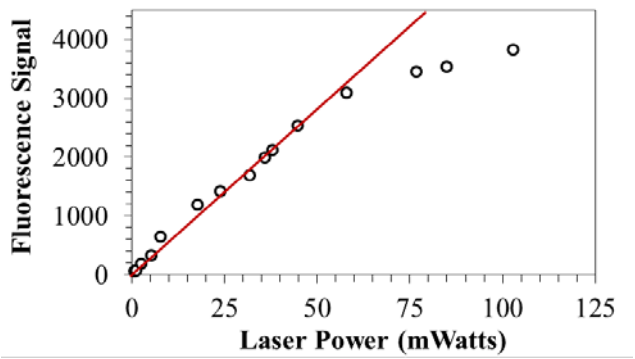

Figure 6: Fluorescence saturation curve for the 624 nm excitation transition of HNO. Fluorescence was collected at 750 nm with its peak fluorescence signal plotted as a function of incident laser power.

HNO FLUORESCENCE: BACKGROUND PRESSURE DEPENDENCE

The fluorescence observed for HNO laser excitation is due to various collisional and radiative relaxation processes. These processes influence the magnitude of the fluorescence signal. Therefore, it is necessary to evaluate the influence of background gas pressure on the resulting fluorescence signal. For these experiments, HAN was injected into the thermal decomposition system at three different temperatures at a constant flow rate (~80 nL/s). The background pressure was adjusted by throttling the vacuum pump valve to obtain a desired total pressure. The resulting fluorescence spectra were numerically integrated with the same procedure used to produce the excitation profiles and plotted as a function of total chamber pressure.

Results shown in figure 7 demonstrate that increasing the background gas pressure can enhance the fluorescence yield up to a pressure of ~500 mTorr. The increased signal can be attributed to increased collisional coupling of HNO from the upper ro-vibrational energy levels into the resulting fluorescence level. At pressures above ~500 mTorr collisional effects likely begin to disperse the energy deposited into the excited ro-vibrational state, resulting in competing relaxation pathways and yielding a net lower fluorescence signal.

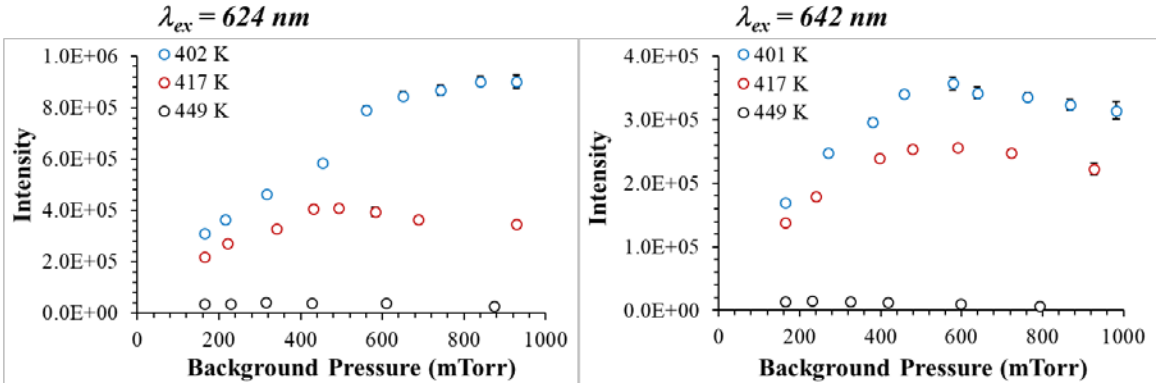

Figure 7: Background pressure dependence on the LIF signal for 624 nm laser excitation (left) and 642 nm laser excitation (right). Three temperature were examined and are color coded.

The dependence of HNO generation on temperature is also illustrated in figure 7. Under similar flow rate and total pressure conditions, increasing the temperature of the system results in a decrease in fluorescence signal. The decrease in fluorescence signal is likely attributed to additional decomposition reaction mechanisms that kinetically compete with the initial formation pathway of HNO detailed in R1-R6. In addition, the highly reactive nature of HNO suggests that

Air Force Office of Scientific Research Grant FA9550-18-1-0442

HNO further reacts to produce additional decomposition species, such as N_2O through HNO dimerization, resulting in a loss mechanism. Future work is required to detail these loss mechanisms and are the subject of ongoing work.

SUMMARY AND CONCLUSIONS

We have presented an initial assessment of the use of laser-induced fluorescence towards the detection of HNO generated from the thermal decomposition of HAN. Two excitation transitions were examined, the first involving the $\tilde{A}^1A'' – X^1A'$ (100 – 000) transition with excitation at 623.8 nm and the second involving the $\tilde{A}^1A'' – X^1A'$ (011 – 000) transition with excitation at 642.3 nm. Each excitation transition examined yielded three spectral regions of fluorescence. For both excitation transitions, the low wavelength fluorescence regime demonstrated a significant broadening of the fluorescence lines which is initially attributed to an HNO pre-dissociation mechanism. The middle fluorescence regime demonstrated the largest fluorescence signal with signals centered at 750 nm and 715 nm for 624 nm and 642 nm excitation, respectively. The high wavelength fluorescence spectral regime showed narrow low intensity signals and would be useful for fundamental diagnostics; however, it is less useful for the analytical detection of HNO.

Assessment of HNO excitation profiles downstream from the decomposition system showed negligible differences in the recorded linewidths regardless of upstream thermal decomposition temperature or background gas pressure. The result of near constant HNO absorption linewidths allows peak fluorescence signals to be directly related to the density of generated HNO. Laser-induced fluorescence saturation curves were also produced and confirmed that the laser system currently used has the ability to optically saturate both laser excitation schemes examined, greatly increasing the system's signal-to-noise ratios. The final assessment of HNO fluorescence was conducted on the background pressure of the system. Results demonstrate that increasing the background gas pressure can enhance the fluorescence yield up to a pressure of ~500 mTorr, after which collisional effects likely begin disperse the energy deposited into the excited ro-vibrations state, resulting in competing relaxation pathways.

The results presented here demonstrate for the first time that laser-induced fluorescence can be utilized to examine the production of HNO from the thermal decomposition of HAN. Fluorescence spectra recorded under identical experimental conditions convincingly demonstrated that both excitation schemes examined here provided excellent signal-to-noise and signal-to-background ratios. The work presented here provides an experimental approach to the sensitive and selective detection of HNO under vacuum conditions which can be applied to a wide range of applications including ionic liquid thermal decomposition.

FUTURE WORK

Ultimately, the goal of this research is to develop a technique that can effectively quantify HNO relative the amount of HAN that is being decomposed. As presented here, laser-induced fluorescence provides a sensitive and selective means to detect HNO under the experimental conditions examined here. Unfortunately, the highly reactivity nature of HNO negates the development of analytical standards for system calibration. Furthermore, the lack of fundamental data on the various HNO transition probabilities involved in the fluorescence schemes presented here makes absolute density calculations from absolute fluorescence radiance measurements difficult and prone to large error.

A solution to this issue may be found with the use of mass spectrometry. As noted previously, electron impact ionization of HNO results in its near complete fragmentation, resulting in the production and subsequent detection of H^+ and NO^+. Thus, quantitative measurements on HNO^+ at m/z = 31 are very difficult and analytically undesirable. Moreover, vaporized nitric acid produced from the thermal decomposition of HAN nearly completely fragments within the ionizer, resulting in a substantial contribution to the amount of NO^+ at m/z = 30. Therefore, a significant chemical interferent exists making quantitative measurements on HNO using the m/z = 30 signal challenging. However, if nitric acid were removed from the system, the resulting signal at m/z =

Air Force Office of Scientific Research Grant FA9550-18-1-0442

30 would be directly related to the amount of HNO generated. Future work will examine the possibility of removing nitric acid from the vapor phase via a gas phase precipitation reaction. A stoichiometrically excess quantity of ammonia, NH_3, vapor will be introduced into the thermal decomposition system. The result will be the formation of an ammonium nitrate precipitate via the following reaction: NH_3 (g) + HNO_3 (g) → NH_4NO_3 (s). The cool surface of the quartz tube immediately following the thermal decomposition system provides a convenient location for the development and removal of ammonium nitrate solid, i.e. removal of nitric acid. A mass spectrometer positioned downstream from the quartz tube will be calibrated with a nitric oxide analytical gas standard. Therefore, the resulting signal at m/z = 30 acquired during the thermal decomposition of HAN, with HNO_3 removed, can be used to quantify the amount of HNO produced. Concurrently, laser-induced fluorescence measurements will be preformed on the system, thus, the fluorescence signal can be directly related to the generation of HNO from the thermal decomposition of HAN. The primary reason for using laser-induced fluorescence over mass spectrometry has to do with the technique's superior selectivity. Under certain operating conditions HAN may produce species which possess a fragment ion at m/z = 30. For example, HONO and N_2O are expected to be produced from the thermal decomposition of HAN, each of which would produce a fragment ion at m/z =30. Laser-induced fluorescence would be immune to the development of these various N-O containing molecular species. Therefore, in order to utilize the mass spectrometer to calibrate the laser-induced fluorescence system for HNO, temperatures and flow rates will be carefully chosen in order to suppress the kinetic development of the aforementioned chemical species. An analytical comparison study between LIF and mass spectrometry will also be assessed.

ACKNOWLEDGMENTS

This work was supported by the Air Force Office of Scientific Research Grant FA9550-18-1-044

REFERENCES

1. Donius, B. R. & Rovey, J. L. Ionic Liquid Dual-Mode Spacecraft Propulsion Assessment. *J. Spacecr. Rockets* **48**, 110–123 (2011).
2. Donius, B. R., Rovey, J. L., Propulsion, C., Agency, I., Nitrate, H., Red, I., Nitric, F., Impulse, S., Tertroxide, N., Pressure, C. C., Dimethylhydrazine, U., Fuming, W., Acid, N. & Hall, T. Analysis and Prediction of Dual-Mode Chemical and Electric Ionic Liquid Propulsion Performance. in *48th AIAA Aerospace Sciences Meeting* AIAA-2010-1328 (2010).
3. Lozano, P., Glass, B. & Martinez-Sanchez, M. Performance characteristics of a linear ionic liquid electrospray thruster. in *29th International Electric Propulsion Conference* IEPC-2005-192 (2005).
4. Lozano, P. & Martinez-sanchez, M. Efficiency Estimation of EMI-BF4 Ionic Liquid Electrospray Thrusters. in *41st AIAA/ASME/SAE/ASEE Joint Propulsion Conference* AIAA-2005-4388 (2005).
5. Lozano, P. & Martínez-Sánchez, M. Ionic liquid ion sources: Suppression of electrochemical reactions using voltage alternation. *J. Colloid Interface Sci.* **280**, 149–154 (2004).
6. Courtney, D. G., Dandavino, S. & Shea, H. Comparing direct and indirect thrust measurements from passively fed ionic electrospray thrusters. *J. Propuls. Power* **32**, 392–407 (2016).
7. Gomez Jenkins, M., Krejci, D. & Lozano, P. CubeSat constellation management using Ionic Liquid Electrospray Propulsion. *Acta Astronaut.* **151**, 243–252 (2018).
8. Lozano, P. C., Martínez-Sánchez, M. & Hruby, V. Electrospray Propulsion. *Encycl. Aerosp. Eng.* 1–12 (2010) doi:10.1002/9780470686652.eae121.
9. Zorzos, A. N. & Lozano, P. C. The use of ionic liquid ion sources in focused ion beam applications. *J. Vac. Sci. Technol. B Microelectron. Nanom. Struct.* **26**, 2097 (2008).
10. Garoz, D., Bueno, C., Larriba, C., Castro, S., Romero-Sanz, I., Fernandez de la Mora, J., Yoshida, Y. & Saito, G. Taylor cones of ionic liquids from capillary tubes as sources of pure ions: The role of surface tension and electrical conductivity. *J. Appl. Phys.* **102**, 064913 (2007).
11. Romero-Sanz, I., Aguirre De Carcer, I. & Fernandez De La Mora, J. Ionic propulsion based on heated Taylor cones of ionic liquids. *J. Propuls. Power* **21**, 239–242 (2005).
12. Romero-Sanz, I., Bocanegra, R., Fernandez de la Mora, J. & Gamero-Castaño, M. Source of heavy molecular ions based on Taylor cones of ionic liquids operating in the pure ion evaporation regime. *J. Appl. Phys.* **94**, 3599–3605 (2003).
13. Shamshina, J. L., Smiglak, M., Drab, D. M., Parker, T. G., Dykes, H. W. H., Di Salvo, R., Reich, A. J. & Rogers, R. D. Catalytic ignition of ionic liquids for propellant applications. *Chem. Commun.* **46**, 8965–7 (2010).
14. Oommen, C., Rajaraman, S., Chandru, R. A. & Rajeev, R. Catalytic Decomposition of Hydroxylammonium Nitrate Monopropellant. *Proc. Int. Conf. Chem. Chem. Process (ICCCP 2011)* **10**, 205–209 (2011).
15. Jankovsky, R. S. Han-based monopropellant assessment for spacecraft. *32nd Jt. Propuls. Conf. Exhib.* (1996) doi:10.2514/6.1996-2863.
16. Farshchi, M., Vaezi, V. & Shaw, B. D. Studies of Han-based monopropellant droplet combustion. *Combust. Sci. Technol.* **174**, 71–97 (2002).
17. Courthéoux, L., Amariei, D., Rossignol, S. & Kappenstein, C. Thermal and catalytic decomposition of HNF and HAN liquid ionic as propellants. *Appl. Catal. B Environ.* **62**, 217–225 (2006).
18. Khare, P., Yang, V., Meng, H., Risha, G. A. & Yetter, R. A. Thermal and electrolytic decomposition and ignition of han-water solutions. *Combust. Sci. Technol.* **187**, 1065–1078 (2015).
19. Lee, H. S. & Litzinger, T. A. Thermal decomposition of han-based liquid propellants. *Combust. Flame* **127**, 2205–2222 (2001).

Air Force Office of Scientific Research Grant FA9550-18-1-0442

20. Lee, H. S. & Litzinger, T. A. Chemical kinetic study of HAN decomposition. *Combust. Flame* (2003) doi:10.1016/S0010-2180(03)00157-3.
21. Lee, Y. J. & Litzinger, T. A. Combustion chemistry of HAN, TEAN, and XM46. *Combust. Sci. Technol.* **141**, 19–36 (1999).
22. Meng, H., Khare, P., Risha, G. A., Yetter, R. A. & Yang, V. Decomposition and ignition of HAN-based monopropellants by electrolysis. *47th AIAA Aerosp. Sci. Meet. Incl. New Horizons Forum Aerosp. Expo.* 1–16 (2009) doi:10.2514/6.2009-451.
23. Oxley, J. & Brower, K. Thermal Decomposition of Hydroxylamine Nitrate. *Proc. SPIE Int. Soc. Opt. Eng.* **0872**, (1988).
24. Berg, S. P. & Rovey, J. L. Decomposition of Monopropellant Blends of Hydroxylammonium Nitrate and Imidazole-Based Ionic Liquid Fuels. *J. Propuls. Power* **29**, 125–135 (2013).
25. Zube, D. M., Wucherer, E. J. & Reed, B. Evaluation of HAN-Based Propellant Blends. in *39th AIAA/ASME/SAE/ASEE Joint Propulsion Converence* AIAA-2003-4643 (2003).
26. Kidd, F. G., Baird, M. J., Neff, G. & Lemmer, K. Experimental Vaporization and Computational Modeling of Ionization of Hydroxylammonium Nitrate in Vacuum. *34th Int. Electr. Propuls. Conf.* (2015).
27. Liu, L., Wei, C., Guo, Y., Rogers, W. J. & Sam Mannan, M. Hydroxylamine nitrate self-catalytic kinetics study with adiabatic calorimetry. *J. Hazard. Mater.* (2009) doi:10.1016/j.jhazmat.2008.06.009.
28. Liu, L., Papadaki, M., Pontiki, E., Stathi, P., Rogers, W. J. & Mannan, M. S. Isothermal decomposition of hydroxylamine and hydroxylamine nitrate in aqueous solutions in the temperature range 80-160 °C. *J. Hazard. Mater.* **165**, 573–578 (2009).
29. Farhat, K., Amariei, D., Batonneau, Y., Kappenstein, C. & Ford, M. Reaction balance of thermal and catalytic decomposition of nitrogen-based ionic monopropellants. *Collect. Tech. Pap. - 43rd AIAA/ASME/SAE/ASEE Jt. Propuls. Conf.* **6**, 6254–6263 (2007).
30. Wei, C., Rogers, W. J. & Mannan, M. S. Thermal decomposition hazard evaluation of hydroxylamine nitrate. in *Journal of Hazardous Materials* (2006). doi:10.1016/j.jhazmat.2005.07.044.
31. Cronin, J. T. & Brill, T. B. Thermal decomposition of energetic materials. 8. Evidence of an oscillating process during the high-rate thermolysis of hydroxylammonium nitrate, and comments on the interionic interactions. *J. Phys. Chem.* **90**, 178–181 (1986).
32. Schoppelrei, J. W. & Brill, T. B. Spectroscopy of hydrothermal reactions. 7. Kinetics of aqueous [NH3OH]NO3at 463-523 K and 27.5 MPa by infrared spectroscopy. *J. Phys. Chem. A* **101**, 8593–8596 (1997).
33. Wang, Q., Wei, C., Pérez, L. M., Rogers, W. J., Hall, M. B. & Mannan, M. S. Thermal decomposition pathways of hydroxylamine: Theoretical investigation on the initial steps. *J. Phys. Chem. A* **114**, 9262–9269 (2010).
34. Jonusas, M. & Krim, L. A possible answer to the mysterious non-detection of hydroxylamine in space: The thermal desorption mechanism. *Mon. Not. R. Astron. Soc.* **459**, 1977–1984 (2016).
35. Izato, Y. I., Koshi, M. & Miyake, A. Initial Decomposition Pathways of Aqueous Hydroxylamine Solutions. *J. Phys. Chem. B* **121**, 4502–4511 (2017).
36. Miranda, K. M. The chemistry of nitroxyl (HNO) and implications in biology. *Coord. Chem. Rev.* **249**, 433–455 (2005).
37. Fukuto, J. M., Switzer, C. H., Miranda, K. M. & Wink, D. A. Nitroxyl (HNO): Chemistry, Biochemistry, and Pharmacology. *Annu. Rev. Pharmacol. Toxicol.* **45**, 335–355 (2005).
38. Zareipour, R. & Vahedpour, M. Atmospheric reaction pathways of methanimine and nitroxyl: a theoretical study. *Struct. Chem.* (2019) doi:10.1007/s11224-019-01375-0.
39. Miller, J. A., Smooke, M. D., Green, R. M. & Kee, R. J. Kinetic Modeling of the Oxidation of Ammonia in Flames. *Combust. Sci. Technol.* **34**, 149–176 (1983).
40. Rafeev, V. A. & Rubtsov, Y. I. Kinetics and mechanism of thermal decomposition of hydroxylammonium nitrate. *Russ. Chem. Bull.* **42**, 1811–1815 (1993).
41. Lozovsky, V. A. & Cheskis, S. Intracavity laser absorption spectroscopy study of HNO in hydrocarbon flames doped with N_2O. *Chem. Phys. Lett.* **332**, 508–514 (2000).

Air Force Office of Scientific Research Grant FA9550-18-1-0442

42. Dalby, F. W. The Spectrum and Structure of the HNO Molecule. *Canadian Journal of Physics* vol. 36 1336–1371 (1958).
43. Bancroft, J. L., Hollas, J. M. & Ramsay, D. A. The Absorption Spectra of HNO and DNO. *Canadian Journal of Physics* vol. 40 322–347 (1962).
44. Pearson, J., Orr-ewing, A. J., Ashfold, M. N. R. & Dixon, R. N. J-dependent linewidths for the (110)-(000) band of the A^1A”-X ^1A‘ transition of HNO studied by cavity ring-down spectroscopy. **92**, 1283–1285 (1996).
45. Dixon, R. N., Noble, M., Taylor, C. A. & Delhoume, M. Magnetic-field and time-resolved studies of the electronic spectrum of HNO. *Faraday Discuss. Chem. Soc.* **71**, 125–142 (1981).
46. R . N . Dixon, G . W . Series & Duxbury, G. . Optical Double Resonance with Laser-Induced Fluorescence Detection. **307**, 603–615 (1982).
47. Mayama, S., Egashira, K. & Obi, K. Laser induced fluorescence of HNO and DNO $\tilde{a}^1A''$ —-X^1A' in a supersonic free jet. *Res. Chem. Intermed.* **12**, 285–302 (1989).
48. Detection of steady state concentration of HNO by photoacoustic spectroscopy.pdf.
49. Faßheber, N., Schmidt, M. C. & Friedrichs, G. Quantitative HNO detection behind shock waves. *Proc. Combust. Inst.* **36**, 607–615 (2017).
50. Weiß, J. & Schinke, R. Renner-Teller induced predissociation of HNO($\tilde{a}^1a''$): Rotational-state dependent linewidths of quasibound states. *J. Chem. Phys.* **115**, 3173–3183 (2001).
51. Pearson, J., Orr-Ewing, A. J., Ashfold, M. N. R. & Dixon, R. N. Spectroscopy and predissociation dynamics of the $\tilde{A}\ ^1A''$ state of HNO. *J. Chem. Phys.* **106**, 5850–5873 (1997).
52. Ten, G. N. & Baranov, V. I. Vibrational Structure of the Absorption Sectra and Model of the HNO and DNO Molecules in the Excited State. **68**, 39–44 (2001).

Air Force Office of Scientific Research Grant FA9550-18-1-0442